MR-based respiratory and cardiac motion correction for PET imaging

Thomas Küstner [a,b,*], Martin Schwartz [a,c], Petros Martirosian [c], Sergios Gatidis [b],
Ferdinand Seith [b], Christopher Gilliam [d], Thierry Blu [d], Hadi Fayad [e], Dimitris Visvikis [e],
F. Schick [c], B. Yang [a], H. Schmidt [b,1], N.F. Schwenzer [b,1]

[a] Institute of Signal Processing and System Theory, University of Stuttgart, Stuttgart, Germany
[b] Department of Radiology, University of Tübingen, Tübingen, Germany
[c] Section on Experimental Radiology, University of Tübingen, Germany
[d] Department of Electronic Engineering, Chinese University of Hong Kong, Hong Kong
[e] INSERM U1101, LaTIM, University of Bretagne, Brest, France

A B S T R A C T

Purpose: To develop a motion correction for Positron-Emission-Tomography (PET) using simultaneously acquired magnetic-resonance (MR) images within 90 s.

Methods: A 90 s MR acquisition allows the generation of a cardiac and respiratory motion model of the body trunk. Thereafter, further diagnostic MR sequences can be recorded during the PET examination without any limitation. To provide full PET scan time coverage, a sensor fusion approach maps external motion signals (respiratory belt, ECG-derived respiration signal) to a complete surrogate signal on which the retrospective data binning is performed. A joint Compressed Sensing reconstruction and motion estimation of the subsampled data provides motion-resolved MR images (respiratory + cardiac). A 1-POINT DIXON method is applied to these MR images to derive a motion-resolved attenuation map. The motion model and the attenuation map are fed to the Customizable and Advanced Software for Tomographic Reconstruction (CASToR) PET reconstruction system in which the motion correction is incorporated. All reconstruction steps are performed online on the scanner via Gadgetron to provide a clinically feasible setup for improved general applicability. The method was evaluated on 36 patients with suspected liver or lung metastasis in terms of lesion quantification (SUVmax, SNR, contrast), delineation (FWHM, slope steepness) and diagnostic confidence level (3-point Likert-scale).

Results: A motion correction could be conducted for all patients, however, only in 30 patients moving lesions could be observed. For the examined 134 malignant lesions, an average improvement in lesion quantification of 22%, delineation of 64% and diagnostic confidence level of 23% was achieved.

Conclusion: The proposed method provides a clinically feasible setup for respiratory and cardiac motion correction of PET data by simultaneous short-term MRI. The acquisition sequence and all reconstruction steps are publicly available to foster multi-center studies and various motion correction scenarios.

© 2017 Elsevier B.V. All rights reserved.

1. Introduction

The hybrid Positron-Emission Tomography (PET) and Magnetic Resonance (MR) technology offers the possibility to combine the high resolution of MR imaging (MRI) with the high molecular sensitivity of PET. This enables simultaneous whole-body data acquisition and fusion of the non-invasive multifunctional MRI with the molecular information of PET.

In the field of oncology, detection and quantification of tumor lesions is an important aim. PET image quality is determined by the amount of measured tracer uptake, which depends on the amount of injected dose, and the acquisition time. Since the amount of injectable dose is limited the acquisition time is chosen in a range of several minutes. During this time period the PET acquisition of the body trunk is affected by motion originating from the patient, mainly respiration and cardiac motion. Any motion between successively measured pairs of photons however leads to a misplacement of the detected PET event and yields a reduced PET quantification and detection rate, i.e. incorrectly estimated uptake, lesion volume and shape. These motion artifacts manifest in

* Corresponding author.
E-mail address: thomas.kuestner@iss.uni-stuttgart.de (T. Küstner).
[1] Authors contributed equally to this work.

the PET image as a spreading along the dominant moving direction (mainly cranio-caudal). Reported cranio-caudal diaphragm displacements caused by respiratory motion are between 10-26mm and up to 75 mm for normal and deep inspiration, respectively (Clifford et al., 2002; Korin et al., 1992; Suramo et al., 1983) with a concomitant non-rigid deformation of adjacent organs such as the lung and liver. The heart is also affinely displaced due to respiration in addition to the complex non-rigid cardiac deformation (Seppenwoolde et al., 2002). Moreover, the respiratory and cardiac motion show a large intra and inter-patient variability (Allen et al., 2004) which demands the need for an adaptive correction technique. Other sources of non-periodic motion such as peristalsis or swallowing contribute additionally, but periodic respiratory and cardiac motion is considered the main source for motion artifacts, especially in thoracic PET.

Given the long acquisition times and the nature of achieving a PET image, prospective or triggered motion correction (MC) procedures are less effective and hence retrospective gating techniques have been dominantly used for minimizing the impact of respiratory motion. The respiratory gating signal can be acquired using external devices such as a respiratory belt or camera (Nehmeh and Erdi, 2008). A dual respiratory and cardiac PET gating using a real-time positioning system and an electro-cardiogram (ECG) device was performed in Lamare et al. (2014). However, the necessity of additionally placed hardware may limit the methods usage in clinical practice and hence it is desirable to build in and derive the gating signal from the acquisition process itself, denoted as self-navigation. The derivation of a gating signal from a simultaneous 4D (3D + time) computer tomography (Ambwani et al., 2011; Fayad et al., 2012) or from the PET data itself (He et al., 2008; Klein et al., 2001; Manber et al., 2015; Paul et al., 2011; Thielemans et al., 2011; Visvikis et al., 2003) has been studied. The increased radiation exposure caused by CT and the limited spatial and temporal resolution of PET images hinder the usability of these approaches in clinical routine. In addition to gating, the non-rigid deformations between different motion states can be compensated by estimating a motion model in one imaging modality (e.g. CT, MR, PET) and applying it intra- or inter-modal (McClelland et al., 2013).

The emergence of simultaneous PET/MR systems offer new possibilities for inter-modal MC in which the non-radiating and non-ionizing MRI is used to correct for motion artifacts in the PET images (Catana, 2015). However, reliable generation of an MR-based motion model depends on motion imaging of free-breathing subjects. These techniques are either based on fast imaging sequences which are often constrained by small field of views (FOV) and/or low spatial/temporal resolution, or on retrospective gating procedures which assume a periodic motion, i.e. inter-cycle motion can hardly be resolved.

For an accurate MC a high-resolution 4D motion model on a Cartesian grid over a large FOV is desired in order to capture all deformations simultaneously. A 4D MR motion model can be generated by the acquisition of repeatedly measured 2D images (Rohlfing et al., 2004; Würslin et al., 2013), high-resolution 3D acquisitions at multiple breath-hold positions (Wang et al., 1996) or low-resolution 3D images under free movement (van Vaals et al., 1993), but such methods lack the possibility to fully capture highly-resolved 3D deformations in short measuring time. Some 3D imaging methods based on non-Cartesian readouts (Chandarana et al., 2011; Feng et al., 2016; 2014; Grimm et al., 2015) have been reported to be less affected by moving objects than Cartesian trajectories, but undesirable off-resonance effects from gradient imperfections and streaking or blurring artifacts due to a Cartesian regridding might occur. Hybrid radial/spiral trajectories with Cartesian readouts (Cheng et al., 2015; Forman et al., 2013; Prieto et al., 2015; Zhu et al., 2015) tend to overcome these issues. Other techniques for motion imaging are based on MR tagging by special

selective RF pulses (Zerhouni et al., 1988) or series of RF pulses (Axel and Dougherty, 1989; Mosher and Smith, 1990) or phase-contrast velocity-encoding (Moran, 1982). However, the derived images have limited usage in diagnostics and the extraction of a reliable motion model can be very challenging. Generally in the reconstruction, from the time-resolved images a motion model is derived which is described as voxel displacement vector fields between the different motion states.

A gating signal relates the motion model with the true underlying motion to be captured. In MRI for respiratory motion tracking, external devices like cameras (Maclaren et al., 2015; Noonan and Howard, 2014) or respiratory belts (Chun et al., 2012) can also be used but require additional hardware placement and just measure a proxy of the breathing. More precise measurements can be obtained by the acquisition of slice-selective navigators (Ehman and Felmlee, 1989), Butterfly navigators (Cheng et al., 2012), Cloverleaf navigators (van der Kouwe et al., 2006) or by self-navigation techniques (Pipe, 1999). The latter example can be incorporated smoothly into the imaging sequence without causing interferences.

The combination of the MR-derived motion model with the PET data for an inter-modal MC can be either image-based or listmode-based (Fayad et al., 2016). An image-based approach uses gated and individually reconstructed PET images which are deformed to a reference state and finally averaged (Fayad et al., 2015b; Grimm et al., 2015; Würslin et al., 2013), whereas listmode-based methods incorporate the motion correction in the PET reconstruction process (Fayad et al., 2015a; Lamare et al., 2007; Manber et al., 2015).

In order to provide a clinically feasible setting, the time required for the MC should be as short as possible to allow the flexibility of acquiring further diagnostic sequences. Previous methods acquired the motion model throughout the complete PET scan time (Grimm et al., 2015; Würslin et al., 2013) or only a fraction of it (Manber et al., 2015). This allows on the one hand a direct matching of the gating signal with the motion model, but on the other hand restricts the MR capabilities to performing MC only. Accelerated acquisition strategies allow for a faster motion model generation, and even dual-gated MC strategies can be incorporated: Dual-gated MC of cardiac PET images under free-breathing has been shown in Würslin et al. (2016) and for respiratory MC of PET images in Rank et al. (2016). However, with the shortening of the acquisition time for MC purposes, one loses the ability to track the underlying motion by the MR-side for the complete PET scan time. Moreover, for a clinically feasible setting, an online MC on the PET/MR scanner is desired to allow for a streamlined integration into the clinical routine protocols and by thus improving general applicability. All previous works so far focused on offline processing of the data.

In this work, we enhance our previous PET/MR MC system (Würslin et al., 2013) by highlighting four aspects. First, we incorporate a 4D Cartesian MR acquisition (Küstner et al., 2017), which subsamples the phase-encoding directions subject to an Enhancing Sharpness by Partially Reduced Subsampling Set (ESPReSSo) subsampling mask (Küstner et al., 2016a), under free-movement conditions. The MR acquisition sequence, including an MR self-navigation signal, is kept as short as possible ($<$ 2min) to reduce the MR occupation for the MC.

For respiratory signal coverage over the complete PET examination time, the second contribution of this work is the usage of a sensor fusion approach. We presented initial results in Küstner et al. (2016b, 2017) which shall be investigated further in this work. An ECG-derived respiration (EDR) signal and data from a respiratory belt are acquired throughout the PET examination. In the sensor fusion, these signals are matched during training to an MR self-navigation signal to serve in an estimation phase as a more reliable respiratory surrogate than the individual signals alone. The ECG signal serves as cardiac surrogate.
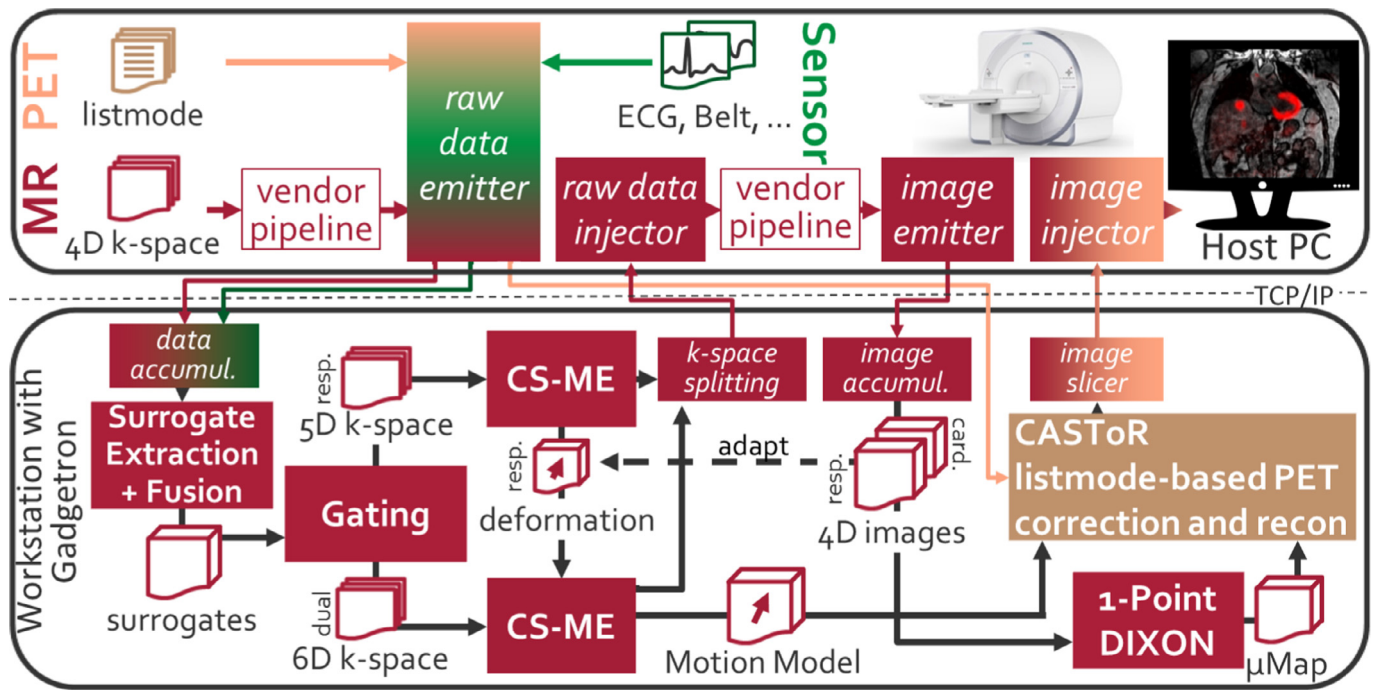
Fig. 1. Proposed respiratory and cardiac motion correction system for a clinical setup via Gadgetron on a whole-body PET/MR scanner. Communication occurs over TCP/IP between the PET/MR host computer and the external workstation hosting the Gadgetron server. The respective data transmitter (emitter, splitting, slicer) and receiver (accumulator, injector) blocks are shown in italic. The Gadgetron server houses the main reconstruction process including the joint Compressed Sensing and motion estimation procedure (CS-ME).

In order to provide a clinical feasible setup and online data processing, the third contribution of this work is the integration of the PET/MR MC system inside Gadgetron (Hansen and Sorensen, 2013). The extracted and fused surrogate signals are used for a retrospective dual gating of the MR data. This subsampled MR data is jointly reconstructed and the motion model estimated (Küstner et al., 2015). For the motion model estimation, we employ an optical flow-based image registration (Gilliam et al., 2016). By means of a 1-point DIXON method (Ma, 2008) the motion state matching attenuation maps are derived. A listmode-based PET reconstruction in which the motion correction is incorporated (Merlin, 2016) yields the final motion-corrected PET image. The acquisition sequence and the Gadgetron reconstruction system are made publicly available.

As a fourth contribution, we evaluate the proposed PET/MR MC system on 36 patients with suspected liver or lung metastasis and investigate the impact of MR scan time shortening for MC.

2. Material and methods

The proposed respiratory and cardiac MC system for a clinical setup via Gadgetron (Hansen and Sorensen, 2013) on a whole-body PET/MR scanner is illustrated in Fig. 1. Respective procedures will be described in the following sections. The reconstructions and motion corrections are carried out on an external workstation connected via network to the PET/MR host computer. The workstation houses the Gadgetron framework to provide sufficient hardware capacity and software flexibility. This architecture layout is invisible to operators using the scanner; they will just be presented with the corrected results on the PET/MR host computer. The vendor-specific reconstruction pipeline is mainly kept untouched to minimize interference and to ensure correct vendor-specific correction methods (e.g. geometric distortion correction). The thereby necessary data emitter and injector modules are depicted in Fig. 1. The temporal acquisition workflow is shown in Fig. 2.

2.1. PET/MR data acquisition

During the first 90 s the MR motion model is recorded with a 3D spoiled T1w gradient-echo sequence (Küstner et al., 2017) simultaneously to the PET data. The remaining MR time is free for diagnostic MR sequences which are usually run for the corresponding PET application. The motion model data in the 3D Cartesian k-space is continuously acquired while the patient is breathing freely. In each repetition time, a fully sampled readout (line in k-space along the k_x direction) for a random combination of phase-encoding k_y and 3D-encoding k_z is acquired based on a compacted variable-density Gaussian probability density function. The compression along one of the phase-encoding directions is according to a so called ESPReSSo mask (Küstner et al., 2016a), which uses a higher sampling density for high frequency components. This results in improved edge delineation in the reconstructed image which is beneficial for the image registration algorithm. Every time T_{Nav} the sequence periodically acquires the central k-space components which serve as an MR self-navigation signal. The time-invariant sampling allows a flexible, retrospective, motion-state assignment of each sample in the gating step (Küstner et al., 2017).

The acquired MR data is sent out over a TCP/IP connection to an external workstation hosting the Gadgetron server on which the reconstruction is carried out (Schwartz et al., 2016).

2.2. Sensor signal acquisition

Additional respiratory and cardiac sensor signals are acquired simultaneously to the MR sequence with the incorporated multi-dimensional MR self-navigation signal. The sole difference is that these external signals cover the complete PET examination time. The cardiac cycles are captured by an ECG signal. Lung volume changes due to breathing cause impedance variations in the ECG electrodes which reflect in a modulation of the ECG signal by the respiration (Pallas-Areny et al., 1989). These modulations can be re-
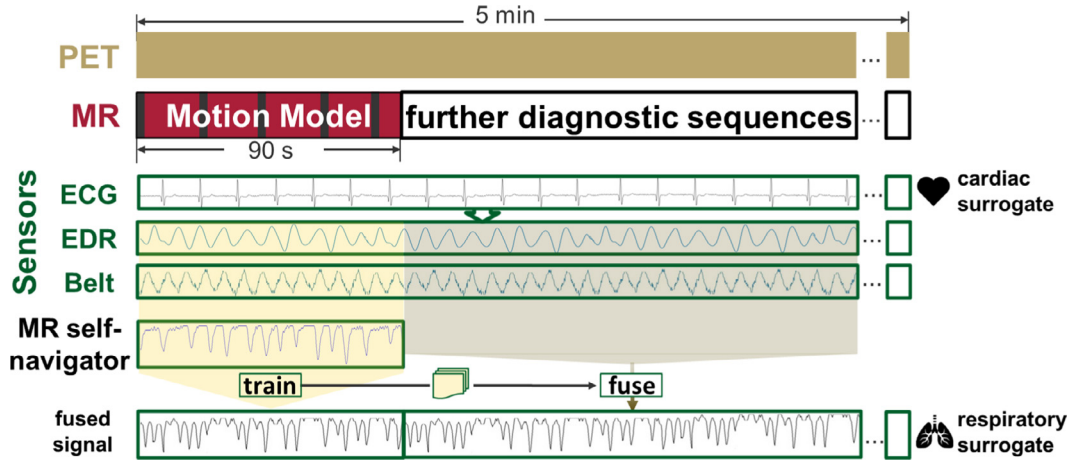
Fig. 2. Acquisition protocol and timeline of the proposed method. A motion model is generated in the first 90 s of the PET bed position freeing time for further diagnostic MR sequences. The external sensor signals are mapped via a sensor fusion approach to a respiratory surrogate signal which spans the complete PET examination time. The respiratory and cardiac surrogates are used in the subsequent gating procedure.

stored yielding an EDR signal (Widjaja et al., 2012). Further respiratory signals can be captured via a respiratory belt or an optical camera system based on a Microsoft Kinect v1 camera (Küstner et al., 2016b). All sensor signals are synchronized via the clock of the scanner host PC.

2.3. Surrogate signal extraction and fusion

The MR self-navigation signal is first extracted from the raw MR data (Küstner et al., 2017). All the external respiratory measurements (EDR, respiratory belt, camera) provide different manifestations of the respiration resulting in distinct accuracies and ambiguities. Since the MR navigator is the best measure for the actual interior displacement of the diaphragm caused by respiration, it should serve as the respiratory surrogate signal on which the gating takes place. However, the MR navigator is just available for the first few minutes of the acquisition. It is not acquired in the remaining time so as not to interfere with the clinical MR protocols. Hence, to ensure a reliable motion model generation and estimation, full PET examination time coverage of the respiratory surrogate signal can be achieved by a sensor fusion approach which maps the respiratory signals onto a synthesized surrogate signal. More information can be found in our previous works (Küstner et al., 2016b; 2017). For the overlap acquisition time of the MR motion model and external sensor signals (training), the signals are split up into overlapping time windows of length L with each of them covering variable portions of the respiratory cycle ranging from half a cycle up to several cycles. After resampling onto a common grid, a feature vector is extracted from each window consisting of amplitude differences, phase offset to first maximum, frequency, slope steepnesses, amount of cycles and wavelet coefficients of symlets. The windows are used to train extended Kalman filters consisting of parameterizable models being able to represent different breathing states: normal, deep, shallow, breath-hold, inhale, exhale, periodic, a-periodic. The employed patient-specific models $m(t, \underline{p})$ with parameters $\underline{p}$ at time points t are a modified raised cosine waveform (MRCW) (Hsieh et al., 2016)

$$m(t, \underline{p}) = \begin{cases} A & , \text{ if } \frac{1}{2f} - T_{a1} < t < \frac{1}{2f} + T_{a2} \\ A\cos\left(\frac{2\pi f}{\beta_1}\left(|t - \frac{1}{2f}| - T_{a1}\right)\right), & \text{ if } T_{b1} < t < \frac{1}{2f} - T_{a1} \\ A\cos\left(\frac{2\pi f}{\beta_2}\left(|t - \frac{1}{2f}| - T_{a2}\right)\right), & \text{ if } \frac{1}{2f} + T_{a2} < t < \frac{1}{f} - T_{b2} \end{cases}$$

$$(1)$$

with: $T_{a1} = \frac{X(1 - \beta_1)}{2f}, T_{b1} = \frac{(1 - X)(1 - \beta_1)}{2f}$ (2)

$$T_{a2} = \frac{X(1 - \beta_2)}{2f}, T_{b2} = \frac{(1 - X)(1 - \beta_2)}{2f}$$ (3)

a Boltzman function

$$m(t, \underline{p}) = \frac{A_1 - A_2}{1 + e^{\frac{t - t_0}{\Delta t}}} + A_2$$ (4)

and a cubic B-Spline model

$$m(t, \underline{p}) = t + \sum_{t_k \in \mathcal{C}} p_k \beta^3\left(\frac{t - t_k}{\sigma}\right)$$ (5)

with control point set $\mathcal{C}$, control grid spacing σ and cubic B-Spline polynomials $\beta^3(\cdot)$. The Kalman filter models and parameters are summarized in Table 1. The states are identified by the kernel PCA (Schölkopf et al., 1997) reduced feature vector. In the reconstruction time period, the same splitting, as in the training, is applied and the trained Kalman filter of the best correlated training signal block is used to perform the mapping. The correlation is found by the minimal Mahalanobis distance in feature space. The output of these fused signals serve as a respiratory surrogate over the complete PET examination time. The ECG signal is acquired throughout the complete PET examination time and serves as a cardiac surrogate signal.

2.4. Gating

With the help of the respiratory and cardiac surrogate signals, each sample can be assigned to a specific motion state. The respiratory gates are placed according to a k-means clustering with possible view sharing $b \in [0, 1]$ ($b = 1 : 50\%$ overlap) amongst neighboring gates. The multichannel 3D MR k-space data is first sorted into a 5D k-space tensor consisting of the spatial, channel and respiratory temporal domain. The cardiac cycles are neglected first to increase sampling efficiency per respiratory gate, because the cardiac motion has only little impact on the respiratory motion, especially in the abdominal region. From this k-space an initial respiratory motion model can be derived in the following joint reconstruction.

The cardiac gates are determined via a modified QRS complex detector with arrhythmia control (Pan and Tompkins, 1985) and possible view sharing. A dual-gating (respiratory and cardiac) is performed with an accompanied through-time filling in the joint

Table 1
Sensor fusion models for Kalman filters of representative breathing states.

States	Model	Parameters
Normal, deep, shallow, breath-hold, inhale, exhale	Modified raised cosine waveform	$\underline{p} = [f, \beta_1, \beta_2, A, X]^T$
Inhale, exhale	Boltzman	$\underline{p} = [A_1, A_2, t_0, \Delta t]^T$
Periodic, a-periodic	Cubic B-Spline	$\underline{p} = [p_1, \ldots, p_M]^T$ with $M = L/\sigma$

reconstruction from other respiratory motion states to a given respiratory reference state based on the initial respiratory motion model.

2.5. Joint reconstruction and motion estimation

The subsampled respiratory and dual-gated k-spaces are independently reconstructed. Instead of a sequential Compressed Sensing (CS) reconstruction and motion estimation (ME), the coupling between the reconstruction of the motion-resolved k-space data and the ME of the reconstructed k-space data can be utilized in a joint iterative reconstruction. An alternating projection between the motion-compensated CS reconstruction and the ME of the currently CS-reconstructed image helps to improve the reconstruction quality and directly delivers the respective deformation field (Küstner et al., 2015).

A regularized Focal Underdetermined System Solver (FOCUSS) algorithm carries out the CS reconstruction of the image ρ from the gated k-space data $\underline{v}$ with an ESPReSSo regularization $\overline{h}_{ESP}(\cdot)$ (Küstner et al., 2016a) to account for the sampling space compactification. A regularization $h_{MC}(\cdot)$ is used for the ME (Küstner et al., 2015) and a regularization for the MR receiver channel weighting $\mathbf{G}$ (Lustig and Pauly, 2010).

$$\text{find } \underline{\rho} = \mathbf{\Psi W} \underline{q} \text{ to } \min_{\underline{q}} \left\| \underline{v} - \mathbf{\Phi F}\tau\,\mathbf{\Psi W}\underline{q} \right\|_2$$
$$+ \lambda_{PI} \left\| (\mathbf{\Psi G} - \mathbf{I})\mathbf{W}\underline{q} \right\|_2$$
$$+ \lambda_S \left\| \underline{q} \right\|_2 + \lambda_{ESP} h_{ESP}\left(\underline{q}\right) + \lambda_{MC} h_{MC}\left(\underline{q}\right)$$

$$\text{with: } h_{ESP}\left(\underline{q}\right) = \left\| (\mathbf{\Phi}\underline{v} + (\mathbf{I} - \mathbf{\Phi})\underline{v}^*) - 0.5 \cdot \mathcal{F}\mathbf{\Psi} \right.$$
$$\left. \cdot \left(\mathbf{W}^*\underline{q}^* \circ e^{2i\arg\left(\mathbf{W}\underline{q}\right)} + \mathbf{W}\underline{q} \right) \right\|_2$$

$$\text{with: } h_{MC}\left(\underline{q}\right) = \left\| \sum_{t, u \in [1, N_G]} \mathbf{\Psi W}\underline{q}_u - \tau_t^u\left(\mathbf{\Psi W}\underline{q}_t\right) \right\|_2 \quad (6)$$

where $\mathbf{W}$ denotes the affine scaling transformation of FOCUSS for the sparse image $\underline{q}$ with a sparsifying Karhunen-Loève transformation $\mathbf{\Psi}$ from the ESPReSSo subsampled Fourier coefficients $\mathbf{\Phi F}$. The spatial-temporal matching τ_t^u between motion-state u and t is considered in τ with a deformation field update by minimizing the residue in the regularization over N_G motion states. The deformation fields are estimated along the temporal directions by a multi-resolution optical-flow based image registration algorithm, called local all-pass (LAP) (Gilliam et al., 2016). Each non-rigid deformation can be modelled as a local rigid displacement which corresponds to linear phase ramps in k-space. These phase modulations can be expressed as local all-pass filter operations, which can be carried out very efficiently and fast, yielding an accurate deformation field.

First the respiratory gated k-space (ignoring the cardiac states) is reconstructed by means of the CS-ME reconstruction to determine the respiratory-resolved MR image and an initial respiratory deformation field. This deformation field is used as a through-time filling of the dual-gated MR data to reconstruct in a second CS-ME a cardiac motion-resolved MR image in a respiratory reference state (e.g. end-expiratory state). The combination of the cardiac and respiratory deformation field yield the overall motion model, see Fig. 1.

2.6. Vendor-specific corrections

Vendor-specific corrections are kept unimpaired to ensure a high MR image quality. This demands, however, more data transmission between the MR host and Gadgetron workstation. For the large FOV, geometric distortions occur at the MR image edges which are corrected in the vendor-pipeline. Therefore, the derived motion model is adapted accordingly by the feedback motion-resolved and vendor-corrected MR images.

2.7. Motion-compensated PET reconstruction

Attenuation maps are directly derived from the matching motion-state T1w MR images based on a 1-point DIXON method (Ma, 2008). The MR images are recorded in the first opposed-phase echo time to support the extraction and to provide a fast acquisition scheme with minimal intra-echo motion. This acquisition strategy prevents the need of an additional DIXON scan at the beginning and a subsequent deformation of the acquired attenuation maps. The attenuation maps and the motion model are provided as input for the listmode-based PET reconstruction, which is implemented in the Customizable and Advanced Software for Tomographic Reconstruction (CASToR) (Merlin, 2016).

A listmode-based motion correction was implemented during PET image reconstruction, allowing the use of all acquired and available data. The motion model (deformation field), extracted as described in the previous section, was incorporated within the one-pass listmode expectation maximization (OPL-EM) algorithm to reconstruct a single motion-compensated PET image, according to previously validated implementation (Fayad et al., 2015b; Lamare et al., 2007).

The standard OPL-EM algorithm can be written as follows:

$$n_j^{k+1} = \frac{n_j^k}{s_j} \sum_{i \in T_k} p_{ij} \frac{1}{q_i^k} \quad \forall k = 1, \ldots, K \quad (7)$$

where

$$q_i^k = \sum_{j=1}^{J} p_{ij} n_j^k \quad (8)$$

is the expected count in line of response (LOR) i, p_{ij} is the purely geometric term representing the geometric probability of detecting at LOR i an event generated in voxel j, n_j is the intensity of voxel j, J is the total number of voxels, s_j is the voxel j of the sensitivity image and K is the number of time subsets k. k is both the iteration number and the number of subset used in that iteration. T_k is the set of listmode events in the kth subset.

The discrete motion model τ can be incorporated into the PET system matrix P, whose elements p_{ij} represent the geometric probability of detecting at LOR i an event generated in voxel j. Thus, the motion compensation incorporated system matrix

$$\mathbf{P}_t = \tau_t^1(\mathbf{P}) \quad (9)$$

accounts for the deformation of the radioactive distribution from time t to the reference time. The standard OPL-EM algorithm in Eq. (8) is subsequently modified to:

$$\underline{n}^{k+1} = \frac{\underline{n}^k}{\mathbf{S}} \circ \sum_{N_G} \mathbf{P}_t^T \frac{1}{\mathbf{P}_t \underline{n}^k} \quad \forall k = 1, \ldots, K \tag{10}$$

where $\mathbf{P}_t^T$ describes the transposed motion compensated system matrix. The sensitivity image $\mathbf{S}$ used for attenuation and normalization correction is produced through a forward-backward projection and was also corrected for motion according to $\mathbf{P}_t$ (Fayad et al., 2015b; Lamare et al., 2007).

3. Experimental evaluation

Datasets of 36 patients (age 60 ± 9 years, 20 female) with suspected liver or lung metastasis were acquired on a 3T whole-body PET/MR scanner (Biograph mMR, Siemens Healthineers, Germany). PET/MR examination followed a routine PET/CT, without repeated radiotracer injection, ~ 120 min after injection of 318 ± 20 MBq of ^{18}F-FDG (22 patients) or 177 ± 31 MBq of ^{68}Ga-DOMITATE (14 patients). The study was approved by the local ethics committee and all patients gave written consent. A 3D-spoiled gradient-echo (GRE) sequence with TE/TR $= 1.23$ ms/2.60 ms, bandwidth $= 890$ Hz/px and a flip angle of $7°$ was used. A matrix size of $256 \times 256 \times 144$ (RO $\times$ PE $\times$ 3D $\Leftrightarrow$ HF $\times$ LR $\times$ AP) was acquired covering a field-of-view of $500 \times 500 \times 360$ mm^3. A 2D MR self-navigation signal ($256 \times 8 \times 1$, RO $\times$ PE $\times$ 3D) was acquired each $T_{\mathrm{Nav}} = 200$ ms. For all patients the respiratory belt and for 12 patients the ECG signal were acquired additionally on a sampling period of 200 ms and 2.60 ms, respectively. The camera signal was not acquired for all patients and is therefore omitted in the following evaluation. PET emission data of one bed position (FOV covering thorax and upper abdomen) were acquired for 5min under free movement (breathing, cardiac motion) in list-mode. The MR sequence was run for the complete PET scan time to allow for a retrospective analysis of the sensor fusion and investigation on motion model reliability versus acquisition time. Due to the random subsampling scheme a retrospective scan time shortening can be performed (Küstner et al., 2017). All presented results were reconstructed from a cropped MR scan of $t = 90$ s, if not stated otherwise. MR data were retrospectively gated into 8 respiratory gates with view-sharing of $b = 1$ and 8 cardiac gates with $b = 0.2$ and afterwards reconstructed with empirically determined Lagrangian multipliers $\lambda_S = 0.1$, $\lambda_{PI} = 0.01$, $\lambda_{ESP} = 0.03$ and $\lambda_{MC} = 0.05$ over 5 image registration resolution levels.

PET images were reconstructed via CASToR in the OPL-EM algorithm with 7 iterations, 7 subsets and a 4mm Gaussian filter kernel. Normalization, attenuation, random and scatter correction functionalities were precomputed by a CASToR plugin for the Biograph mMR. All displayed PET images are shown as PET activity concentration (PAC) in [Bq/ml].

The MR acquisition sequence and the Gadgetron reconstruction are publicly available: https://sites.google.com/site/kspaceastronauts/motion-correction/pet-mr-motion-correction

3.1. Sensor fusion

In the first $t = 90$ s the sensor fusion method was trained and applied to the remaining time window of 210s. The respiratory surrogate was extracted from the EDR as well as from the belt signal for the whole examination time. The sensor fusion of the respiratory surrogate was investigated by means of relative deviation on the TR sampling rate between the estimated surrogate and the MR self-navigation signal which serves as ground truth. For comparison both signals were scaled into a range of 0–1, i.e. an absolute

deviation larger than $1/N_G = 0.125$ corresponds to a gate change for equidistant placed gate centroids.

3.2. PET evaluation

The uncorrected, corrected and end-expiratory and systolic gated PET data was examined in a blinded fashion. Regions of interest (ROI) were drawn in the axial slice of maximal intensity for at least one lesion per patient with a maximal number of 10 examined lesions by a reader experienced in hybrid imaging (N.S. 10 years of experience).

Lesion quantification was determined by maximum standardized uptake value (SUVmax), signal-to-noise ratio (SNR), contrast to lung as well as to blood-pool. The SNR is defined as the ratio between SUVmax and standard deviation in the same ROI. The contrasts were defined as ratios between SUVmax in a ROI to SUVmean of a reference ROI in the lung and heart, respectively.

Line profiles through the lesions in head-feet (HF), anterior-posterior (AP) and left-right (LR) direction provide a measure for lesion delineation by the full-width at half maximum (FWHM) and the slope steepness of this lesion. Boxplots show the mean, median, standard deviation around mean, 25%–75% percentile and outliers over all patients as percentage improvements of the corrected to uncorrected, corrected to reference state gated (end-expiratory, systolic) and uncorrected to gated PET images.

Diagnostic confidence was examined for each lesion by scoring on a 3-point Likert scale (from confident to doubtful).

3.3. Motion model

For two exemplary patients with a periodic and an aperiodic breathing pattern over the PET examination time different motion models were determined. The effect of these motion models on the correction of the PET data was evaluated by means of line profile analysis. The cardiac cycles for all examined patients were approximately periodic and their impact on the motion models was thus not investigated. Motion model stability was examined for retrospective cropping of the MR scan time from $t = 300$ s down to $t = 60$ s in 60 s steps. Reliability of the motion model was examined by the derivation of a motion model from the first 90s of the scan in comparison to a motion model derived from the last 90s of the scan. Furthermore, for two patients the impact of the dual motion-correction (respiratory and cardiac) to a respiratory-only motion-correction is analyzed.

4. Results

Exemplary PET/MR images and derived attenuation maps of an ^{18}F-FDG patient and a ^{68}Ga-DOMITATE patient in Fig. 3 illustrate the improvements on the PET image quality in terms of delineation and quantification as identifiable in the line profiles through a moving lesion in the liver. The MR image quality of the short scan time in Figs. 3–6 is sufficient to derive a reliable motion model. For longer MR acquisition times the motion model remain fairly similar for periodically breathing patients as shown in Fig. 5 and Supplementary Fig. 1. This fact can also be derived from the absolute displacement of the motion model in Fig. 5 and Supplementary Fig. 1 mapping from end-expiratory to end-inspiratory state in the central coronal slice. For aperiodic breathing patient still a reliable motion model can be retrieved, see Fig. 6 and Supplementary Fig. 2.

For a tracer uptake near or in the heart, a dual gating and motion correction (respiratory and cardiac) might be beneficial as illustrated in Fig. 4.

The good alignment between the MR self-navigation signal (if acquired throughout the complete PET examination) and the res-
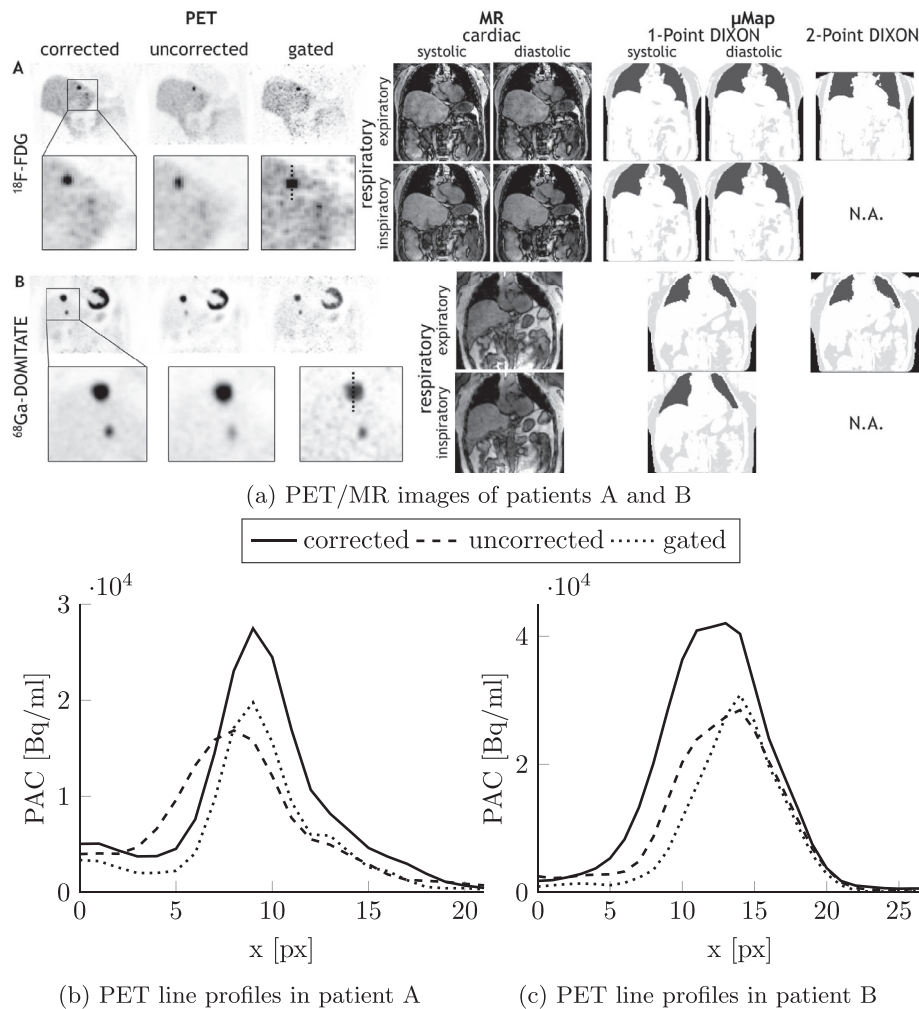
(a) PET/MR images of patients A and B

(b) PET line profiles in patient A

(c) PET line profiles in patient B

Fig. 3. (a) Exemplary PET/MR images and attenuation maps of a melanoma patient A injected with 337MBq ^{18}F-FDG and a neuroendocrine tumor patient B injected with 184 MBq ^{68}Ga-DOMITATE. The 1-POINT DIXON method retrieved motion-state aligned attenuation maps are shown in comparison to the attenuation map acquired of a 2-POINT DIXON scan in breath-hold. (b,c) Line profiles in corrected (——), uncorrected (- - -) and end-expiratory and systolic gated (······) PET image through a moving liver lesion indicate the improvements achieved in patient A by respiratory and cardiac or in patient B by respiratory-only motion correction.

piratory surrogate is depicted in Fig. 7. The Bland–Altman plot in Fig. 8 displays the result of the sensor fusion in relation to the MR self-navigation signal over all samples and patients. 98.4% of the surrogate samples fall into the same gate as if performed on the MR self-navigation signal, i.e. only a small amount of samples lead to an incorrect motion state assignment.

In total, 134 malignant lesions were found and examined in 30/36 patients (83%). For the remaining 6 patients the motion correction could also be conducted, but no malignant lesions were found and thus these patients were excluded from the analysis. In 8 patients more than 10 liver lesions were observed. Overall 116 liver lesions and 18 lung lesions were determined. Percentage improvements of the ROI and line profile values are presented in Fig. 9 over all examined moving lesions in the patient study. Comparison between the corrected and uncorrected PET images showed an overall improvement in terms of quantification (SUVmax: 25%, SNR: 10%, contrast: 27%) and delineation (FWHM: 28%, slope steepness: 99%). Similar findings can be drawn between the corrected and gated PET images for SUVmax, SNR, contrast, FWHM and slope steepness, but with less improvement (7%, 17%, −1%, 17%, 42%, respectively). Both motion correction and gating highly reduced the negative motion effects. However, the lesions of the motion-corrected PET images can be evaluated with a markedly higher diagnostic confidence than the gated ones (5 vs. 64 doubt-

ful lesions) and with a slightly higher confidence than the uncorrected lesions (11 doubtful lesions) as depicted in Fig. 10. This indicates the superiority of motion correction over gating or lacking correction.

5. Discussion

The application of an inter-modality motion correction is of special interest for PET/MR imaging. We propose the usage of a fast acquisition scheme (Küstner et al., 2017) to enable a clinically feasible setup for a respiratory and cardiac motion correction during the entire examination. The proposed MR sequence is able to capture the occurring deformations in a short scan time leaving free acquisition time for further diagnostic sequences. The retrieved image quality is sufficient to determine a motion model as depicted in Figs. 3, 5 and 6 for the correction of the PET image. The MR image quality is determined by the acquisition time, the number of motion states and the underlying motion behaviour of the patient. The optimal tradeoff between these parameters and their impact on the derived image is examined in more detail in Küstner et al. (2017). For an acquisition time of 90 s and sufficient motion resolvability, 8 respiratory and 8 cardiac gates were chosen. Moreover, the reconstruction parameters were empirically chosen and
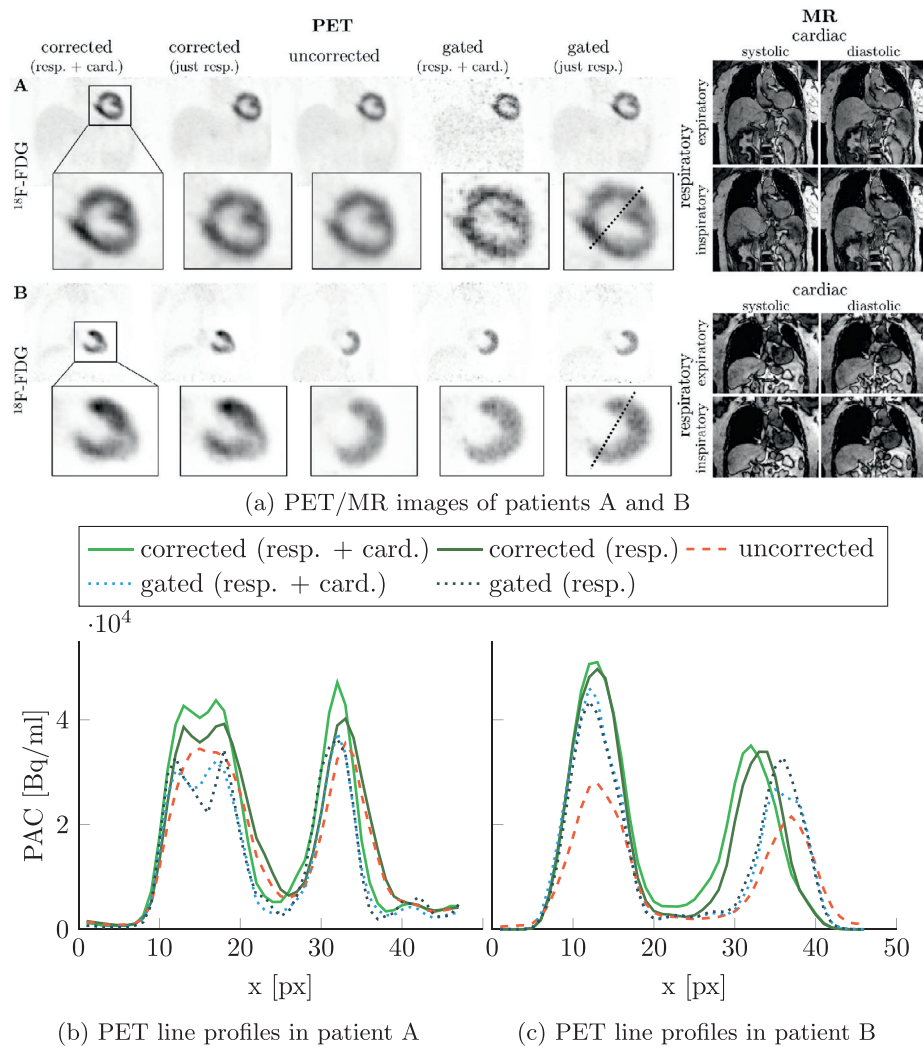
(a) PET/MR images of patients A and B

(b) PET line profiles in patient A

(c) PET line profiles in patient B

Fig. 4. Respiratory and cardiac gating and motion correction in comparison to respiratory-only for two exemplary patients (A and B) with tracer uptake in myocardium. (a) PET/MR images for different motion corrections. Gated PET images are displayed for end-expiratory and systolic position. (b,c) The line profiles along the short axis show the achieved improvements by a dual motion correction in contrast to a gating or respiratory-only correction/gating.

showed a stable convergence behaviour for different settings, refer to Küstner et al. (2015) for more information.

The displayed PET/MR images and line profiles in Fig. 3 reveal the improvements for moving lesions as well as the overall image quality. Additionally, our attenuation maps which were generated by the 1-Point DIXON method from the 4D data match the corresponding motion states and do not need any deformation via a motion model, making an additional scan for an attenuation map obsolete. The scanner generated 2-Point DIXON attenuation map is usually acquired in an end-expiratory breath-hold and hence other motion states need to be reconstructed by applying respective deformations.

A dual gating and correction of the respiratory- and cardiac-induced motion can be beneficial for heart examinations as depicted in Fig. 4. As shown for larger non-rigid deformations, motion correction is superior to gating. The majority of patients included in this study had suspected liver or lung metastasis and none of them had any abnormality in the heart. Thus, a diagnostic improvement by a cardiac motion correction could not be anticipated. Moreover, in oncologic exams, patient's preparation aims at fasting for several hours which in most cases leads to a decreased FDG-uptake in the myocardium. Most of the patients had no or a heterogeneous myocardial uptake. Thus, the full scope of a

dual correction could only be assessed in two patients. We assume that the main influencing factor for tissue deformation around the heart seems to be due to respiration, as e.g. illustrated in Fig. 4. Therefore, only minor visual and quantitative improvements were achieved by cardiac motion correction with the largest benefits for lesions in the near proximity of the heart or for cardiac uptakes. Further studies are required to fully explore the benefits and improvements by a dual (respiratory + cardiac) motion correction in a variety of clinical issues.

In PET, lesion delineation was clearly enhanced and quantification was facilitated. As depicted in Fig. 9, the FWHM and slope steepness of the moving lesions were improved yielding a more accurate lesion placement by correction of motion-induced lesion blurring. The largest deformation correction was achieved in the cranio-caudal direction (HF). However, due to the number of liver and lung metastasis examined, there was also a significant deformation in the anterior-posterior and the left-right direction; such metastasis are able to undergo non-rigid deformation rather than pure linear displacement. Thus performing a non-rigid motion correction helps to improve the delineation in all three spatial directions. In contrast to a pure PET gating, the delineation was further improved due to the sharper and higher lesion uptake as indicated by the enhanced SUVmax. Additionally, improved lesion
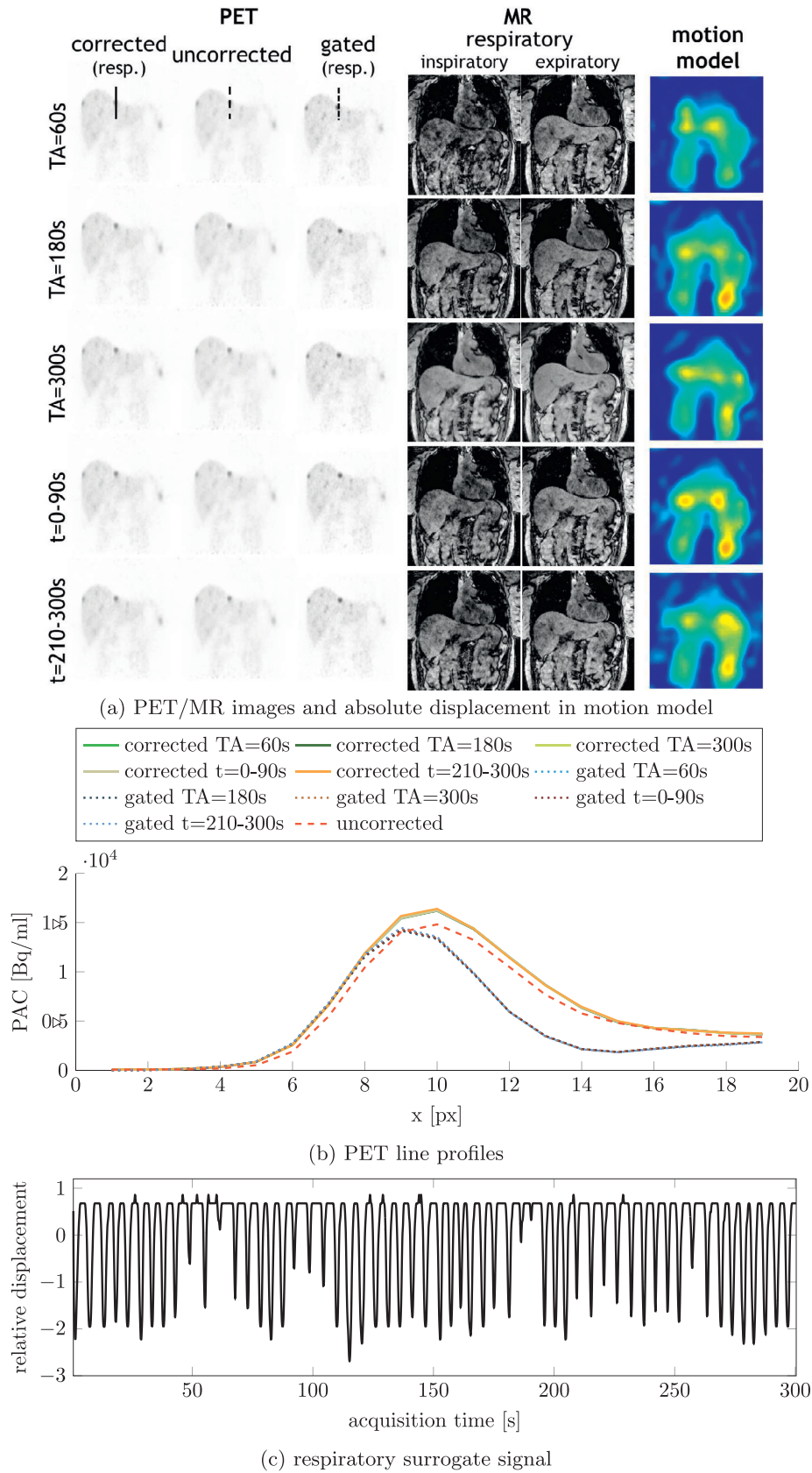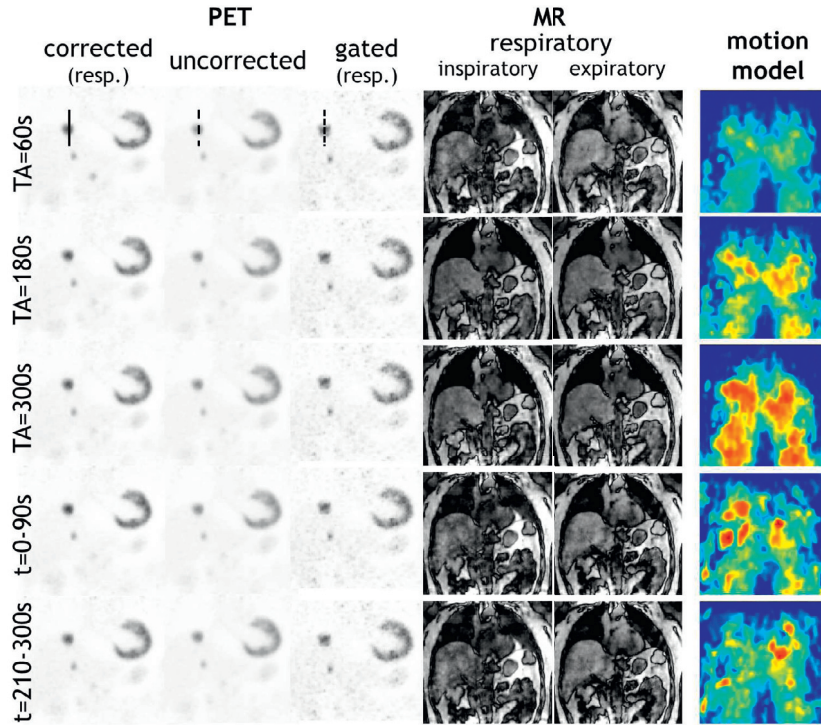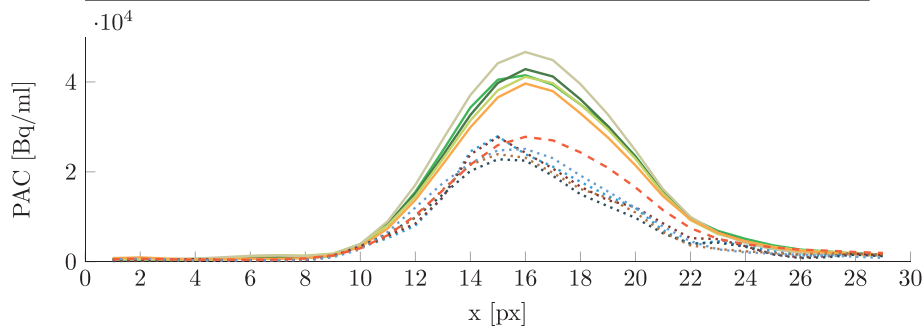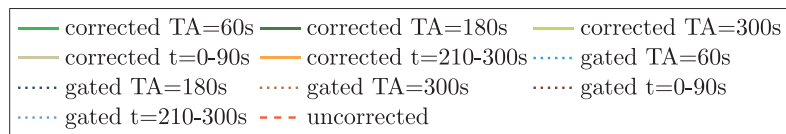
(a) PET/MR images and absolute displacement in motion model

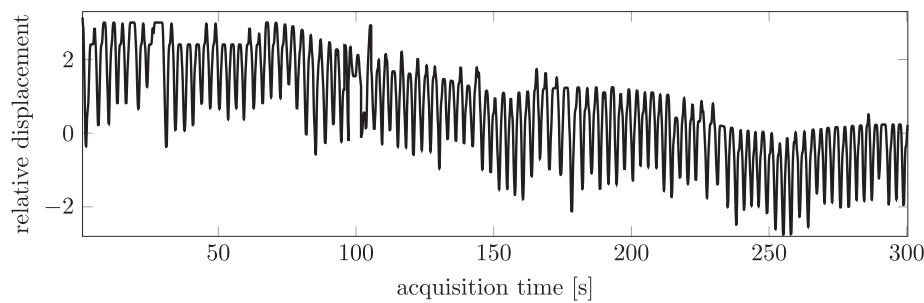(b) PET line profiles

(c) respiratory surrogate signal

Fig. 5. Periodic breathing patient: Motion models derived from the first 60 s, 180 s, 300 s and for the first 90 s and last 90 s of the PET bed position. (a) Respiratory-only corrected, uncorrected and end-expiratory gated PET images with inspiratory and expiratory MR images as well as root-sum-of-squares absolute displacement in all three spatial directions in a central coronal slice are shown. (b) Line profiles through a moving lesion (as indicated in PET images of TA=60 s) in PET images show the consistency amongst different acquisition times. (c) Extracted respiratory surrogate signal. See Supplementary Fig. 1 for all time points.

(a) PET/MR images and absolute displacement in motion model

(b) PET line profiles

(c) respiratory surrogate signal

Fig. 6. Aperiodic breathing patient: Motion models derived from the first 60 s, 180 s, 300 s and for the first 90 s and last 90 s of the PET bed position. (a) Respiratory-only corrected, uncorrected and end-expiratory gated PET images with inspiratory and expiratory MR images as well as root-sum-of-squares absolute displacement in all three spatial directions in a central coronal slice are shown. (b) Line profiles through a moving lesion (as indicated in PET images of TA=60 s) in PET images show the consistency amongst different acquisition times. (c) Extracted respiratory surrogate signal. See Supplementary Fig. 2 for all time points.
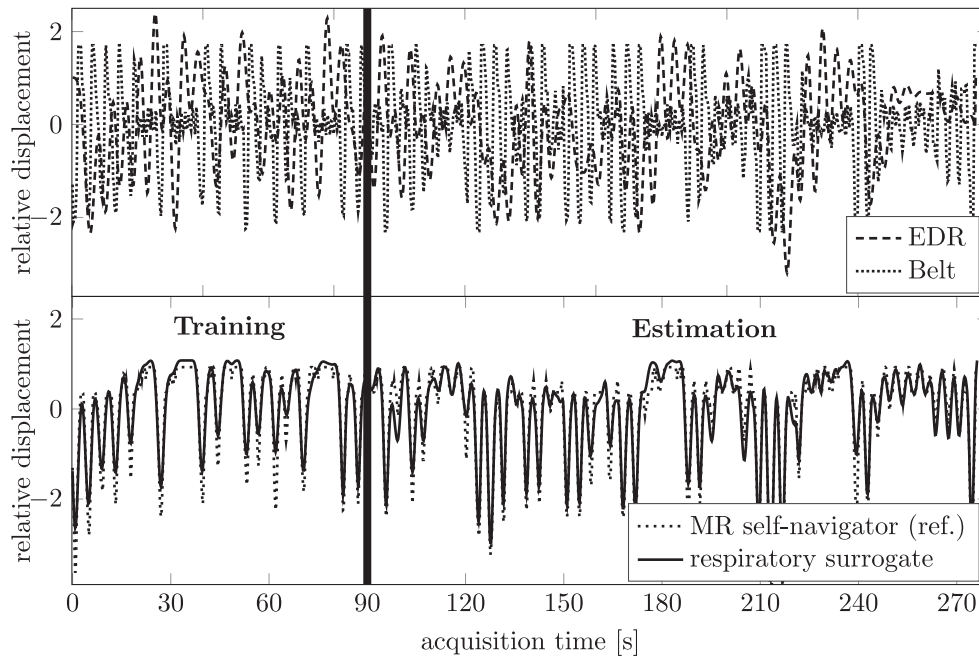
Fig. 7. Exemplary external sensor signals (EDR, respiratory belt; top row) of a patient on which the sensor fusion approach is trained in the first 90 s (Training) and applied afterwards for the whole duration of 280 s (Estimation). The MR self-navigation signal is acquired throughout the complete examination time and serves as comparable reference for the respiratory surrogate signal.
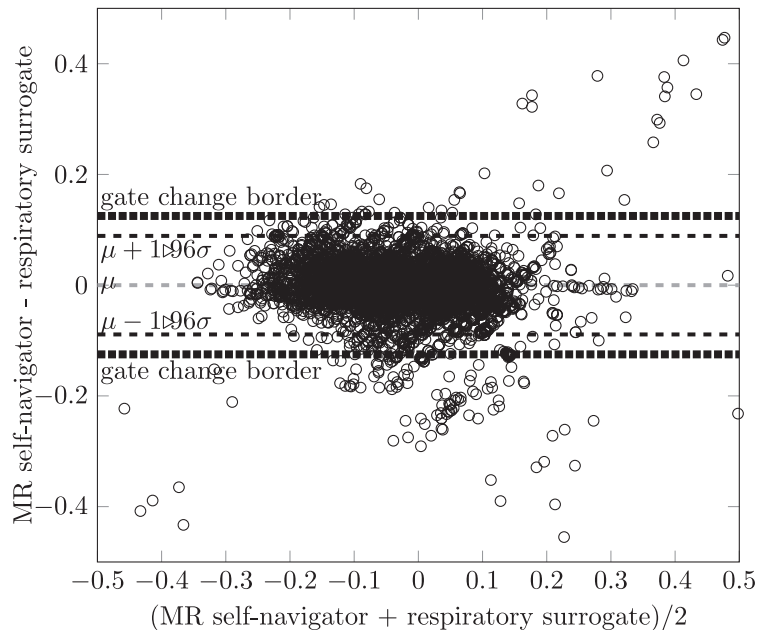

Fig. 8. Bland-Altman plot of the correspondence between the MR self-navigation signal and the respiratory surrogate signal on a sample basis comparison over all 36 patients with mean $\mu = 0$ and deviation $\mu \pm 1.96\sigma = \pm 0.09$. The gate change border is determined by $1/N_G = 0.125$. Outliers are leading to misclassification into a different respiratory motion state.

quantification (SUVmax, SNR, contrast) was also achieved using motion correction compared to PET gating. For contrast measurements, a large ROI was placed in the lung and blood pool to mitigate any varations in the SUVmean. This resulted in fairly similar SUVmean for the corrected and gated PET images. The improved SUVmax in the corrected PET images yielded a slight contrast enhancement in comparison to gating. However, as demonstrated by the radiologists' diagnostic confidence in Fig. 10, the lower SNR in the gated PET images makes visual delineation of lesion significantly more difficult when compared to the corrected images. For the correct-uncorrected comparison, the corrected images obtained an improved contrast than the uncorrected ones, which is particularly beneficial for the detection of small moving lesions. The location and number of the outliers (points above the 75% quantile mark) indicate that motion correction can lead to even greater improvements for some lesions. If no correction is performed, some lesions are severely affected as indicated by the outliers below the 25% quantile mark for the uncorrected-gated comparison. Note that our previously published results (Würslin et al., 2013) demonstrated similar trends however the use of the 3D motion capturing, instead of a 2D method, lead to larger improvements.
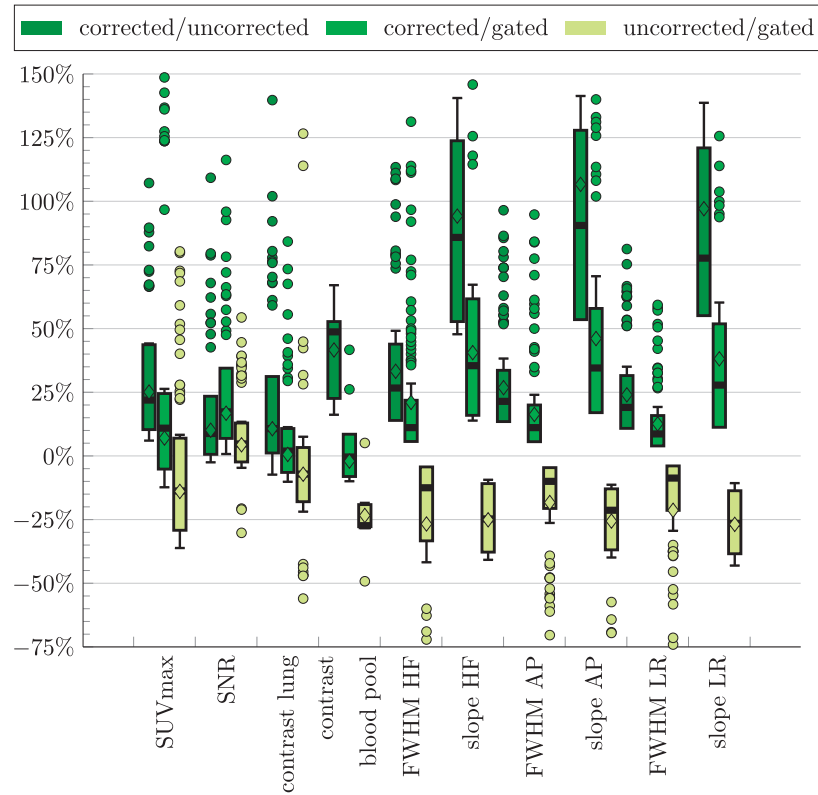
Fig. 9. Percentage improvements for all 134 examined lesions in 36 patients of corrected to uncorrected, corrected to gated (end-expiratory, systolic) and uncorrected to gated PET images. Lesion quantification was assessed by SUVmax, SNR and contrast of examined ROI and delineation by FWHM and slope steepness in line profile along head-feet (HF), anterior-posterior (AP) and left-right (LR) direction. Boxplots indicate the 25% and 75% percentile, median (-), average (◇), standard deviation (whiskers) and outliers (dots).
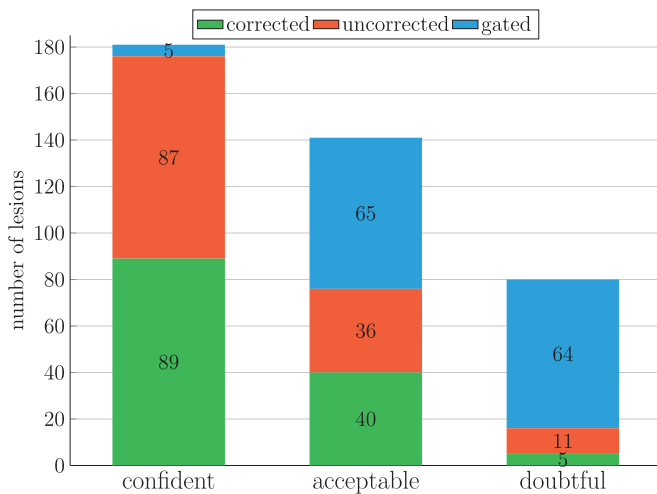

Fig. 10. Diagnostic confidence level of radiologist for lesion depiction in the corrected, uncorrected and gated (end-expiratory, systolic) PET images.

Depending on the underlying motion behavior of the patient, a reliable correction can be conducted. However, due to the retrospective gating of the MR data and the per motion-state discretized deformation field, intra- and inter-cycle variations cannot be tracked in full detail (King et al., 2012) so errors in the PET correction due to displacement of the LOR can occur. Aperiodic behaviors can be captured to a certain degree, e.g. linearly decreasing trend in diaphragm position. For the examined patients a fairly constant heartrate was observed, whereas significant changes

in the respiratory cycle occurred more frequently. For a periodic breathing as shown in Fig. 5 and Supplementary Fig. 1, the cropping of the acquisition time or the selection of the motion model acquisition in the first or last 90 s of the PET bed position does not severely influence the retrieved motion model. Similar deformation fields can be obtained as illustrated by the root-sum-of-squares absolute displacement of all three spatial directions in a central coronal slice which allow to conclude reliabilty of the motion model generation step. It should be considered here that the dominant movement is in head-feet direction. An overestimation of the motion can be observed in the liver, spleen and adjacent anatomical structures such as colon which smoothes out for longer MR acquisitions or in the last 90s acquisition of the PET bed position. The influence of the acquisition time/position on the selection of the reference motion state (end-expiratory and systolic) was found negligible. Minor increases in noise and subsampling-related artifacts can be observed for shorter measuring times, but a good MR image quality can still be retrieved as many samples contribute to the reference state. For the end-inspiratory position, a good MR image can still be reconstructed but with a stronger influence of subsampling-related artifacts as observed in Fig. 5. However, for all acquisition times/positions a similar PET correction was obtained as indicated by the plotted line profile through a dominant moving lesion in which the corrected line profiles coincide. Since still the complete PET data from the 5min scan is available for the gated PET image, the coinciding gated line profiles indicate that the MR-based gating placement provides the same end-expiratory and systolic motion-state for varying acquisition lengths.

For an aperiodic breathing behavior as depicted in Fig. 6 and Supplementary Fig. 2 the motion models are more distinctive for changing acquisition times/positions than the ones shown in

Fig. 5 and Supplementary Fig. 1. The retrieved MR image quality however is still sufficient for a reliable motion model generation. Thus, the corrected PET image quality after applying the varying motion models is not severely affected. In a central coronal slice, a line profile in head-feet direction through a moving lesion exhibits a little bit more variations for the corrected or gated PET images in comparison to Fig. 5, but shows the same behavior. Hence, the retrieved ROI and line profile metrics do not differ substantially. This observation also holds for other moving lesions from this patient. These results originate from the fairly similar periodicity of the breathing cycle with just a difference in the respiratory baseline. Although this reproducibility may not hold for any arbitrary breathing behavior, for all examined patients in this study fairly similar PET results could be obtained for varying MR acquisition times/positions (remark: the PET duration was not cropped). Therefore, the validity of the assumption for a periodic motion needs to be further examined in future studies. In circumstances with more severe aperiodicities a motion model adaption based on the respiratory surrogate as suggested by Baumgartner et al. (2016) might be beneficial.

The MR-derived motion model was validated on the improvements obtained in the PET image, i.e. cross-modality validation, with the hypothesis of PET uptake increase and sharpened delineation for moving lesions. This prooved to be a more trustworthy measure than similarity or overlaps in the MR image alone (same modality). This circumstance is also discussed by Rohlfing (2012). Moreover, we also conducted phantom experiments (Würslin et al., 2014) and validated the LAP image registration on constant and synthetic displacements (Gilliam et al., 2016) which showed similar reliable results.

The retrieved respiratory and cardiac surrogates allow reliable motion model estimation. For complete PET examination time coverage, the external sensor signals are mapped via a sensor fusion approach to a full surrogate signal. This allows an interference-free acquisition of further diagnostic sequences. Instead of solely relying on the external sensor signals this mapping provides a more accurate estimation and omits the shortcomings of the external sensors, e.g. clipping of the respiratory belt signal or over-/underestimations in the EDR. If two or more external sensors are used, possible time gaps or inaccuracies can be overcome, compare the correction of over- and undershoots of the EDR signal in Fig. 7. The marked differences between the sensor signals to the MR self-navigation signal (reference) and between themselves demand a mapping based on defined motion states to enable the generation of a reliable respiratory signal. Any temporal behaviour in the estimation phase which is not available in the training period can not (or only partially) be handled. It is therefore important to provide stable models which can deal with this circumstance. Moreover, the Kalman filter provides in such cases a good tradeoff between signal prediction based on model and observations. In this study we observed mainly the same signal behaviours during training and estimation. In future studies it might be however interesting to learn a representative model over all patients to be able to model all circumstances.

The ECG signal was acquired throughout the complete PET examination time. Thus, the investigation was focused on the sensor fusion of the respiratory signals. Nevertheless, it shall be noted that the sensor fusion concept is also directly applicable to cardiac signals, e.g. mapping the ECG signal to a cardiac self-navigation signal (Kolbitsch et al., 2014; Pang et al., 2014). The retrieved EDR and respiratory belt signal carry enough distinctive information to produce a stable respiratory surrogate. The surrogate and reference MR self-navigator signals show a high matching accordance with small fluctuations. In 98.4% of the cases the samples are binned into the same motion state as demonstrated in Fig. 8. Due to time restrictions and patient compliance, it was not always feasible to acquire an ECG signal. In the future, it is therefore desirable to reduce the dependency on external sensor placement by e.g. using a cardiac self-gating (Kolbitsch et al., 2014; Pang et al., 2014), preinstalled camera systems (Maclaren et al., 2015) or pilot tone navigators (Schroeder et al., 2016).

The streamlined processing via Gadgetron enables a clinically feasible environment in which the operating user is just presented with the corrected results. The operator does not need to care about data handling and correction which makes the proposed system easy to use.

6. Conclusions

We propose a system to perform respiratory and cardiac PET motion correction with a motion model derived from a simultaneously acquired MR data. The MR sequence workload for the motion model generation is kept short to enable the flexibility of acquiring further diagnostic MR sequences, which are usually performed for each PET bed position. In order to provide motion model coverage for the whole PET examination time, we propose a sensor fusion approach to estimate a complete respiratory surrogate signal. The acquired MR data is retrospectively gated and a joint CS-ME reconstruction provides a motion model and a motion-resolved MR image. From this MR image the corresponding attenuation map is extracted via a 1-point DIXON method and applied to a PET listmode-based reconstruction and motion correction. An average PET improvement after motion correction in lesion quantification (SUVmax, SNR, contrast) of 22% and delineation (FWHM, slope steepness) of 64% was achieved compared to the uncorrected PET. All reconstruction steps are carried out online on the scanner via Gadgetron with the vendor-specific correction steps kept intact. This enables an easy handling in a clinical environment. The proposed method is publicly available to foster multi-center studies and various motion correction scenarios.

Supplementary material

Supplementary material associated with this article can be found, in the online version, at 10.1016/j.media.2017.08.002

References

Allen, A.M., Siracuse, K.M., Hayman, J.A., Balter, J.M., 2004. Evaluation of the influence of breathing on the movement and modeling of lung tumors. Int. J. Radiat. Oncol. Biol. Phys. 58 (4), 1251–1257. http://dx.doi.org/10.1016/j.ijrobp.2003.09.081.

Ambwani, S., Karl, W.C., Tawakol, A., Pien, H., 2011. Joint cardiac and respiratory motion correction and super-resolution reconstruction in coronary PET/CT. In: IEEE International Symposium on Biomedical Imaging: From Nano to Macro, pp. 1702–1705.

Axel, L., Dougherty, L., 1989. MR imaging of motion with spatial modulation of magnetization. Radiology 171 (3), 841–845. doi:10.1148/radiology.171.3.2717762.

Baumgartner, C.F., Kolbitsch, C., McClelland, J.R., Rueckert, D., King, A.P., 2016. Autoadaptive motion modelling for MR-based respiratory motion estimation. Med. Image Anal. 35, 83–100. doi:10.1016/j.media.2016.06.005.

Catana, C., 2015. Motion correction options in PET/MRI. Semin. Nucl. Med. 45 (3), 212–223. doi:10.1053/j.semnuclmed.2015.01.001.

Chandarana, H., Block, T.K., Rosenkrantz, A.B., Lim, R.P., Kim, D., Mossa, D.J., Babb, J.S., Kiefer, B., Lee, V.S., 2011. Free-breathing radial 3D fat-suppressed T1-weighted gradient echo sequence: a viable alternative for contrast-enhanced liver imaging in patients unable to suspend respiration. Invest. Radiol. 46 (10), 648–653. doi:10.1097/RLI.0b013e31821eea45.

Cheng, J.Y., Alley, M.T., Cunningham, C.H., Vasanawala, S.S., Pauly, J.M., Lustig, M., 2012. Non-rigid motion correction in 3D using autofocusing with localized linear translations. Magn. Reson. Med. 68 (6), 1785–1797. doi:10.1002/mrm.24189.

Cheng, J.Y., Zhang, T., Ruangwattanapaisarn, N., Alley, M.T., Uecker, M., Pauly, J.M., Lustig, M., Vasanawala, S.S., 2015. Free-breathing pediatric MRI with nonrigid motion correction and acceleration. J. Magn. Reson. Imaging 42 (2), 407–420. doi:10.1002/jmri.24785.

Chun, S.Y., Reese, T.G., Ouyang, J., Guerin, B., Catana, C., Zhu, X., Alpert, N.M., El Fakhri, G., 2012. MRI-based nonrigid motion correction in simultaneous PET/MRI. J. Nucl. Med. 53 (8), 1284–1291. doi:10.2967/jnumed.111.092353.

Clifford, M.A., Banovac, F., Levy, E., Cleary, K., 2002. Assessment of hepatic motion secondary to respiration for computer assisted interventions. Comput. Aided Surg. 7 (5), 291–299. doi:10.3109/10929080209146038.

Ehman, R.L., Felmlee, J.P., 1989. Adaptive technique for high-definition MR imaging of moving structures. Radiology 173 (1). doi:10.1148/radiology.173.1.2781017. 255–63

Fayad, H., Lamare, F., Merlin, T., Visvikis, D., 2016. Motion correction using anatomical information in PET/CT and PET/MR hybrid imaging. Q. J. Nucl. Med. Mol. Imaging 60 (1), 12–24.

Fayad, H., Odille, F., Schmidt, H., Würslin, C., Küstner, T., Feblinger, J., Visvikis, D., 2015a. The use of a generalized reconstruction by inversion of coupled systems (GRICS) approach for generic respiratory motion correction in PET/MR imaging. Phys. Med. Biol. 60 (6), 2529–2546. doi:10.1088/0031-9155/60/6/2529.

Fayad, H., Pan, T., Pradier, O., Visvikis, D., 2012. Patient specific respiratory motion modeling using a 3D patient's external surface. Med. Phys. 39 (6), 3386–3395. doi:10.1118/1.4718578.

Fayad, H., Schmidt, H., Würslin, C., Visvikis, D., 2015b. Reconstruction-Incorporated respiratory motion correction in clinical simultaneous PET/MR imaging for oncology applications. J. Nucl. Med. 56 (6), 884–889. doi:10.2967/jnumed.114.153007.

Feng, L., Axel, L., Chandarana, H., Block, K.T., Sodickson, D.K., Otazo, R., 2016. XD-GRASP: Golden-angle radial MRI with reconstruction of extra motion-state dimensions using compressed sensing. Magn. Reson. Med. 75 (2), 775–788. doi:10.1002/mrm.25665.

Feng, L., Grimm, R., Block, K.T., Chandarana, H., Kim, S., Xu, J., Axel, L., Sodickson, D.K., Otazo, R., 2014. Golden-angle radial sparse parallel MRI: combination of compressed sensing, parallel imaging, and golden-angle radial sampling for fast and flexible dynamic volumetric MRI. Magn. Reson. Med. 72 (3), 707–717. doi:10.1002/mrm.24980.

Forman, C., Grimm, R., Hutter, J.M., Maier, A., Hornegger, J., Zenge, M.O., 2013. Free-breathing whole-heart coronary MRA: motion compensation integrated into 3D cartesian compressed sensing reconstruction. Med. Image Comput. Comput. Assist. Interv. 16 (Pt 2). 575–82

Gilliam, C., Küstner, T., Blu, T., 2016. 3D motion flow estimation using local all-pass filters. In: IEEE International Symposium on Biomedical Imaging (ISBI), pp. 282–285. doi:10.1109/ISBI.2016.7493264.

Grimm, R., Furst, S., Souvatzoglou, M., Forman, C., Hutter, J., Dregely, I., Ziegler, S.I., Kiefer, B., Hornegger, J., Block, K.T., Nekolla, S.G., 2015. Self-gated MRI motion modeling for respiratory motion compensation in integrated PET/MRI. Med. Image Anal. 19 (1), 110–120. doi:10.1016/j.media.2014.08.003.

Hansen, M.S., Sorensen, T.S., 2013. Gadgetron: an open source framework for medical image reconstruction. Magn. Reson. Med. 69 (6). doi:10.1002/mrm.24389. 1768–76

He, J., O'Keefe, G.J., Gong, S.J., Jones, G., Saunder, T., Scott, A.M., Geso, M., 2008. A novel method for respiratory motion gated with geometric sensitivity of the scanner in 3D PET. IEEE Trans. Nucl. Sci. 55 (5), 2557–2565. doi:10.1109/TNS.2008.2001187.

Hsieh, C.H., Chiu, Y.F., Shen, Y.H., Chu, T.S., Huang, Y.H., 2016. A UWB radar signal processing platform for real-Time human respiratory feature extraction based on four-Segment linear waveform model. IEEE Trans. Biomed. Circuits Syst. 10 (1), 219–230. doi:10.1109/TBCAS.2014.2376956.

King, A.P., Buerger, C., Tsoumpas, C., Marsden, P.K., Schaeffter, T., 2012. Thoracic respiratory motion estimation from MRI using a statistical model and a 2-D image navigator. Med. Image Anal. 16 (1), 252–264. doi:10.1016/j.media.2011.08.003.

Klein, G.J., Reutter, B.W., Botvinick, E.H., Budinger, T.F., Huesman, R.H., 2001. Fine-scale motion detection using intrinsic list mode PET information. In: Proceedings IEEE Workshop on Mathematical Methods in Biomedical Image Analysis (MMBIA 2001), pp. 71–78. doi:10.1109/MMBIA.2001.991701.

Kolbitsch, C., Prieto, C., Schaeffter, T., 2014. Cardiac functional assessment without electrocardiogram using physiological self-navigation. Magn. Reson. Med. 71 (3). doi:10.1002/mrm.24735. 942–54

Korin, H.W., Ehman, R.L., Riederer, S.J., Felmlee, J.P., Grimm, R.C., 1992. Respiratory kinematics of the upper abdominal organs: a quantitative study. Magn. Reson. Med. 23 (1), 172–178. doi:10.1002/mrm.1910230118.

van der Kouwe, A.J., Benner, T., Dale, A.M., 2006. Real-time rigid body motion correction and shimming using cloverleaf navigators. Magn. Reson. Med. 56 (5), 1019–1032. doi:10.1002/mrm.21038.

Küstner, T., Würslin, C., Gatidis, S., Martirosian, P., Nikolaou, K., Schwenzer, N.F., Schick, F., Yang, B., Schmidt, H., 2016. MR image reconstruction using a combination of compressed sensing and partial fourier acquisition: ESPResso. IEEE Trans Med Imaging 35 (11), 2447–2458. doi:10.1109/tmi.2016.2577642.

Küstner, T., Würslin, C., Schmidt, H., Yang, B., 2015. Combining Compressed Sensing with motion correction in acquisition and reconstruction for PET/MR. In: IEEE International Conference on Acoustics, Speech and Signal Processing (ICASSP), pp. 788–792. doi:10.1109/ICASSP.2015.7178077.

Küstner, T., Würslin, C., Schwartz, M., Fayad, H., Merlin, T., Gilliam, C., Blu, T., Martirosian, P., Schick, F., Yang, B., Schmidt, H., Schwenzer, N.F., 2017. Motion Correction on a human PET/MR scanner: Clinical feasibility of a motion correction system in patients - an update report. In: Proceedings of the ISMRM, p. 781.

Küstner, T., Würslin, C., Schwartz, M., Martirosian, P., Gatidis, S., Brendle, C., Seith, F., Schick, F., Schwenzer, N.F., Yang, B., Schmidt, H., 2017. Self-navigated 4D cartesian imaging of periodic motion in the body trunk using partial k-space compressed sensing. Magn. Reson. Med. 78 (2), 632–644. doi:10.1002/mrm.26406.

Küstner, T., Würslin, C., Schwartz, M., Martirosian, P., Gatidis, S., Nikolaou, K., Schick, F., Yang, B., Schwenzer, N.F., Schmidt, H., 2016. Simultaneous in-vivo respiratory and cardiac motion correction system for PET/MR. In: Proceedings of the ISMRM, p. 782.

Lamare, F., Le Maitre, A., Dawood, M., Schafers, K.P., Fernandez, P., Rimoldi, O.E., Visvikis, D., 2014. Evaluation of respiratory and cardiac motion correction schemes in dual gated PET/CT cardiac imaging. Med. Phys. 41 (7). doi:10.1118/1.4881099.

Lamare, F., Ledesma Carbayo, M.J., Cresson, T., Kontaxakis, G., Santos, A., Le Rest, C.C., Reader, A.J., Visvikis, D., 2007. List-mode-based reconstruction for respiratory motion correction in PET using non-rigid body transformations. Phys. Med. Biol. 52 (17), 5187–5204. doi:10.1088/0031-9155/52/17/006.

Lustig, M., Pauly, J.M., 2010. SPIRiT: iterative self-consistent parallel imaging reconstruction from arbitrary k-space. Magn. Reson. Med. 64 (2), 457–471. doi:10.1002/mrm.22428.

Ma, J., 2008. A single-point dixon technique for fat-suppressed fast 3D gradient-echo imaging with a flexible echo time. J. Magn. Reson. Imaging 27 (4), 881–890. doi:10.1002/jmri.21281.

Maclaren, J., Aksoy, M., Bammer, R., 2015. Contact-free physiological monitoring using a markerless optical system. Magn. Reson. Med. 74 (2), 571–577. doi:10.1002/mrm.25781.

Manber, R., Thielemans, K., Hutton, B.F., Barnes, A., Ourselin, S., Arridge, S., O'Meara, C., Wan, S., Atkinson, D., 2015. Practical PET respiratory motion correction in clinical PET/MR. J. Nucl. Med. 56 (6), 890–896. doi:10.2967/jnumed.114.151779.

McClelland, J.R., Hawkes, D.J., Schaeffter, T., King, A.P., 2013. Respiratory motion models: a review. Med. Image Anal. 17 (1), 19–42. doi:10.1016/j.media.2012.09.005.

Merlin, T., 2016. Customizable and advanced software for tomographic reconstruction (castor).

Moran, P.R., 1982. Physical constraints in the optimization of medical imaging filters for maximum signal-to-Noise ratio. IEEE Trans. Med. Imaging 1 (3), 197–204. doi:10.1109/TMI.1982.4307573.

Mosher, T.J., Smith, M.B., 1990. A DANTE tagging sequence for the evaluation of translational sample motion. Magn. Reson. Med. 15 (2), 334–339. doi:10.1002/mrm.1910150215.

Nehmeh, S.A., Erdi, Y.E., 2008. Respiratory motion in positron emission tomography/computed tomography: A Review. Semin. Nucl. Med. 38 (3), 167–176. http://dx.doi.org/10.1053/j.semnuclmed.2008.01.002.

Noonan, P.J., Howard, J., 2014. Repurposing microsoft kinect for motion correction in the MRI environment. In: ISMRM Workshop on Motion Correction in MRI, p. 13. Tromsoe, Norway

Pallas-Areny, R., Colominas-Balague, J., Rosell, F.J., 1989. The effect of respiration-induced heart movements on the ECG. IEEE Trans. Biomed. Eng. 36 (6), 585–590. doi:10.1109/10.29452.

Pan, J., Tompkins, W., 1985. A real-time QRS detection algorithm. IEEE Trans. Biomed. Eng. 32 (3). 230–6

Pang, J., Sharif, B., Fan, Z., Bi, X., Arsanjani, R., Berman, D.S., Li, D., 2014. ECG And navigator-free four-dimensional whole-heart coronary MRA for simultaneous visualization of cardiac anatomy and function. Magn. Reson. Med. 72 (5), 1208–1217. doi:10.1002/mrm.25450.

Paul, J.S., Michael, J.O., Paul, K.M., 2011. Extension of a data-driven gating technique to 3D, whole body PET studies. Phys. Med. Biol. 56 (13), 3953.

Pipe, J., 1999. Motion correction with PROPELLER MRI: application to head motion and free-breathing cardiac imaging. Magn. Reson. Med. 42 (5). 963–9

Prieto, C., Doneva, M., Usman, M., Henningsson, M., Greil, G., Schaeffter, T., Botnar, R.M., 2015. Highly efficient respiratory motion compensated free-breathing coronary MRA using golden-step cartesian acquisition. J. Magn. Reson. Imaging 41 (3), 738–746. doi:10.1002/jmri.24602.

Rank, C.M., Heußer, T., Wetscherek, A., Freitag, M.T., Schlemmer, H., Kachelrieß, M., 2016. Respiratory motion compensation for simultaneous PET/MR using strongly undersampled MR data. In: Proceedings of the ISMRM, p. 4249.

Rohlfing, T., 2012. Image similarity and tissue overlaps as surrogates for image registration accuracy: widely used but unreliable. IEEE Trans. Med. Imaging 31 (2), 153–163. doi:10.1109/TMI.2011.2163944.

Rohlfing, T., Maurer, C.R., O'Dell, W.G., Zhong, J., 2004. Modeling liver motion and deformation during the respiratory cycle using intensity-based nonrigid registration of gated MR images. Med. Phys. 31 (3), 427–432. doi:10.1118/1.1644513.

Schölkopf, B., Smola, A., Müller, K.-R., 1997. Kernel Principal Component Analysis. Springer Berlin Heidelberg, Berlin, Heidelberg. 583–588. doi:10.1007/BFb0020217.

Schroeder, L., Wetzl, J., Maier, A., Lauer, L., Bollenbeck, J., Fenchel, M., Speier, P., 2016. A novel method for contact-free cardiac synchronization using the pilot tone navigator. In: Proceedings of the ISMRM, 410, p. 410.

Schwartz, M., Küstner, T., Würslin, C., Martirosian, P., Schwenzer, N.F., Schick, F., Yang, B., Schmidt, H., 2016. Image reconstruction system for compressed sensing retrospective motion correction for the application in clinical practice. In: Proceedings of the ISMRM, p. 1845.

Seppenwoolde, Y., Shirato, H., Kitamura, K., Shimizu, S., van Herk, M., Lebesque, J.V., Miyasaka, K., 2002. Precise and real-time measurement of 3D tumor motion in lung due to breathing and heartbeat, measured during radiotherapy. Int. J. Radiat. Oncol. Biol. Phys. 53 (4), 822–834. doi:10.1016/s0360-3016(02)02803-1.

Suramo, I., Pivnsalo, M., Myllyl, V., 1983. Cranio-caudal movements of the liver, pancreas and kidneys in respiration. Acta Radiol. Diagn. 25 (2), 129–131.

Thielemans, K., Rathore, S., Engbrant, F., Razifar, P., 2011. Device-less gating for PET/CT using PCA. In: 2011 IEEE Nuclear Science Symposium Conference Record, pp. 3904–3910. doi:10.1109/NSSMIC.2011.6153742.

van Vaals, J.J., Brummer, M.E., Dixon, W.T., Tuithof, H.H., Engels, H., Nelson, R.C., Gerety, B.M., Chezmar, J.L., den Boer, J.A., 1993. "Keyhole" method for accelerating imaging of contrast agent uptake. J. Magn. Reson. Imaging 3 (4). 671–5

Visvikis, D., Barret, O., Fryer, T., Turzo, A., Lamare, F., Rest, C.C.L., Bizais, Y., 2003. A posteriori respiratory motion gating of dynamic PET images. In: IEEE Nuclear Science Symposium Conference Record, 5, pp. 3276–3280. doi:10.1109/NSSMIC.2003.1352596.

Wang, Y., Rossman, P.J., Grimm, R.C., Riederer, S.J., Ehman, R.L., 1996. Navigator-echo-based real-time respiratory gating and triggering for reduction of respiration effects in three-dimensional coronary MR angiography. Radiology 198 (1), 55–60. doi:10.1148/radiology.198.1.8539406.

Widjaja, D., Varon, C., Dorado, A.C., Suykens, J.A., Van Huffel, S., 2012. Application of kernel principal component analysis for single-lead-ECG-derived respiration. IEEE Trans. Biomed. Eng. 59 (4), 1169–1176. doi:10.1109/tbme.2012.2186448.

Würslin, C., Fleischmann, D., Bammer, R., 2016. Efficient 5D imaging of thorax and abdomen for MR-guided PET motion correction. In: Proceedings of the ISMRM, p. 881.

Würslin, C., Küstner, T., Bartel, S., Schwenzer, N.F., Yang, B., Schmidt, H., 2014. A simple-to-build and cost-efficient mr-compatible phantom for the simulation of non-rigid motion. In: Proceedings of the ISMRM Motion Correction in MRI Workshop, p. 23. Tromsø, Norway.

Würslin, C., Schmidt, H., Martirosian, P., Brendle, C., Boss, A., Schwenzer, N.F., Stegger, L., 2013. Respiratory motion correction in oncologic PET using T1-weighted MR imaging on a simultaneous whole-body PET/MR system. J. Nucl. Med. 54 (3), 464–471. doi:10.2967/jnumed.112.105296.

Zerhouni, E.A., Parish, D.M., Rogers, W.J., Yang, A., Shapiro, E.P., 1988. Human heart: tagging with MR imaging–a method for noninvasive assessment of myocardial motion. Radiology 169 (1), 59–63. doi:10.1148/radiology.169.1.3420283.

Zhu, Y., Guo, Y., Lingala, S.G., Marc Lebel, R., Law, M., Nayak, K.S., 2015. GOCART: GOlden-angle CArtesian randomized time-resolved 3D MRI. Magn. Reson. Imaging doi: 10.1016/j.mri.2015.12.030 [Epub ahead of print]. http://dx.doi.org/10.1016/j.mri.2015.12.030.

Thomas Küstner received the degree Dipl.-Ing. in Electrical Engineering and Information Technology from the University of Stuttgart, Germany, in 2012. He joined the Institute of Signal Processing and System Theory, University of Stuttgart, Germany and the Department of Radiology, University Hospital of Tübingen, Germany in 2013 as a PhD candidate. His research focuses on PET/MR motion correction, fast acquisition techniques and the accompanied reconstruction methods. Furthermore, he is working on MR image analysis to establish assisting model observers.

Martin Schwartz received the M.Sc. degree in Electrical Engineering and Information Technology from the University of Stuttgart, Germany, in 2015. He joined the Section on Experimental Radiology, University Hospital of Tübingen, Germany and the Institute of Signal Processing and System Theory, University of Stuttgart, Germany in 2015. His current research interests include image post-processing in the field of diffusion-weighted MR imaging and online MR image reconstruction methods.

Petros Martirosian received his physics diploma from the University of Jerewan, Armenia in 1985. From 1985 to 1989, he was a researcher for the physics institute of Jerewan, Armenia in the spectrometry group. Since 2000 he is with the Section of Experimental Radiology at the University of Tübingen, Germany. In 2010 he received his Ph.D. degree. His research interest include MR perfusion imaging of extracranial organs, magnetization transfer MR imaging and whole heart MRI.

Sergios Gatidis is resident physician at the Department of Radiology of the University Hospital of Tübingen where he is currently attached to the MRI research group. He studied Medicine and Mathematics at the University of Tübingen. His field of research lies in the development of techniques for the automated analysis of multiparametric imaging data.

Ferdinand Seith, MD, B.Sc. received the degree "B.Sc." in economic sciences and "MD" from the University of Leipzig, Germany, in 2010 and 2011, respectively. He joined the Department of Radiology, University Hospital of Tübingen, Germany in 2013 as a resident. His research focuses on PET/MR, attenuation correction, motion correction and multiparametric oncologic imaging.

Christopher Gilliam is a Postdoctoral Fellow in the Image and Video Processing Group, Department of Electronic Engineering at The Chinese University of Hong Kong. He graduated from Imperial College London with a First Class Honours MEng in Electrical and Electronic Engineering in 2008 and with a PhD in Electrical and Electronic Engineering in 2013. His research interests include sampling theory; approximation theory and its connection to the sampling of parametric non-bandlimited signals; and motion estimation from image sequences.

Thierry Blu received a "Diplôme d'ingénieur" from École Polytechnique (1986), from Télécom Paris/ENST (1988), as well as a PhD in electrical engineering from ENST (1996). Between 1998 and 2007, he was with the Biomedical Imaging Group at the Swiss Federal Institute of Technology (EPFL) in Lausanne, Switzerland. Since 2008, he has been a Professor in the Department of Electronic Engineering, The Chinese University of Hong Kong. Dr. Blu was the recipient of two best paper awards from the IEEE Signal Processing Society (2003 and 2006). He is also coauthor of a paper that received a Young Author best paper award (2009) from the same society. He was elected Fellow of the IEEE in 2012 for "fundamental contributions to approximation theory in signal and image processing". His research interests include: approximation and sampling theory, image restoration, biomedical imaging, optics and wave propagation.

Hadi Fayad has an initial engineering formation in computer sciences (2006), a master (2007) and a PhD in medical image processing (2011). He was recruited as an assistant professor (2012) at the faculty of medicine at the University of Western Brittany (UBO) and incorporated the LaTIM laboratory (INSERM U1101). His actual research activities deals with motion management in radiotherapy and in multi-modality imaging such as PET/CT and PET/MR. Hadi Fayad is in charge of the SIBM (Signal and Image in Biology and Medicine) master and is responsible for the computer and internet certificate at the faculty of Medicine of the UBO.

Dimitris Visvikis is a director of research with the National Institute of Health and Medical Research (INSERM) in France and a co-director of the Medical Image Processing Lab in Brest (LaTIM, UMR1101). His current research interests focus on improvement in PET/CT image quantitation for specific oncology applications, such as response to therapy and radiotherapy treatment planning, through the development of methodologies for detection and correction of respiratory motion, 4D PET image reconstruction, tumour volume segmentation and activity distribution characterisation algorithms, as well as the development and validation of Monte Carlo simulations for radiotherapy treatment dosimetry applications.

Fritz Schick is Head of the Section of Experimental Radiology at the University Hospital of Tübingen, Germany. He studied medicine and physics at Eberhard-Karls-Universität Tübingen from where he graduated in medicine in 1989 and in physics in 1990. Since 2001, he has a permanent professorship as the Head of the Section of Experimental Radiology at the University of Tübingen. Since 2010 he also leads the Section Metabolic Imaging of the Paul-Langerhans-Institute for Diabetes Prevention in Tübingen.

Bin Yang received the Dipl.-Ing. and Ph.D. degree in 1986 and 1991 from the Ruhr University Bochum, Germany in electrical engineering. From 1996 to 2001, he was a senior researcher on mobile communications at Infineon Technologies, Germany. He is currently the head of the Institute for Signal Processing and System Theory at the University of Stuttgart, Germany. His research interest includes methods and algorithms of statistical signal processing and machine learning. The current focus of his research addresses applications of medical signal processing, radar signal processing, power monitoring, and sensor fusion.

Holger Schmidt is physicist at the Department of Radiology at University Hospital of Tübingen, Germany. He studied Physics at the University of Bonn, Germany and obtained his PhD in Biochemistry at the Science Centre in Jülich, Germany, focusing on nuclear magnetic resonance spectroscopy of biomolecules in structural biology. After his post-doc at the Max-Planck-Institute in Göttingen, Germany, he moved to Tübingen and is now working on simultaneous PET/MR imaging. His main research focus is the implementation of functional and fast MR imaging methods into PET/MR diagnostics, analysis of multiparametric data using multivariate methods as well as MR-based correction techniques for PET imaging.

Nina F. Schwenzer is Senior Radiologist and Assistant Professor at the Diagnostic and Interventional Radiology, Dept. of Radiology at the University of Tübingen. She obtained her Medical Doctorate degree and her post-graduate training in Radiology from the University of Tübingen. For several years she was affiliated to the Section on Experimental Radiology in Tübingen (Head: Prof. Fritz Schick) with the focus of research on fat quantification and clinical applications of arterial spin labeling as well as diffusion weighted MR imaging. Since 2010 she has a research assignment for the clinical evaluation of the PET/MR systems in Tübingen. Since 2011, she works on clinical aspects of hybrid PET/MR imaging at the whole-body PET/MR system and the correlation of functional MRI with PET-parameters for oncological applications in abdominal imaging.